Proceedings of the 4th World Congress on Mechanical, Chemical, and Material Engineering (MCM'18)
Madrid, Spain – August 16 – 18, 2018
Paper No. HTFF 174
DOI: 10.11159/htff18.174

Sediment Erosion Prediction for a Francis Turbine Based on Liquid-Solid Flow Simulation Using Modified PANS

Edgar Cando[1,2], RenFang Huang[1], Esteban Valencia[2] and XianWu Luo[1],*
[1]Department of Energy and Power Engineering, Tsinghua University
Beijing 100084, China
edgar.cando@epn.edu.ec; hrenfang@yeah.net
[2]Departamento de Ingeniería Mecánica, Escuela Politécnica Nacional
Quito 17-01-2759, Ecuador
esteban.valencia@epn.edu.ec; luoxw@tsinghua.edu.cn* corresponding author

Abstract - A challenge in the prediction of the sediment erosion is the proper estimation of the motion and velocity of the solid particles, where Reynolds average Navier-Stokes (RANS) methods show limited resolution to determine the motion of solid phase affected by flow fluctuations. The present study adopts a modified partially averaged-Navier Stokes (PANS) method to analyse the sediment erosion prediction for Francis turbines. Numerical simulations were carried out to obtain liquid-solid two-phase flow information in entire flow passage of a Francis turbine using Eulerian-Lagrangrian approach. The hydraulic performance such as efficiency and discharge of the turbine achieved experimentally, are used to validate the present simulation method. The results show that the modified PANS model can improve the prediction accuracy and the smallest unresolved-to-total ratio of turbulence kinetic energy, f_k, decided with the consideration of the difference between local average grid size and smallest grid size shows a slight accuracy improvement. Based on the two-phase flow field, sediment erosion was predicted in stay vane, guide vane and runner using a semi-empirical equation obtained from an erosion experiment of liquid-solid flow. It is noted that higher physical resolution captured by the turbulence model causes a diminution of the sediment erosion predicted. Further, the numerical simulation reveals that sediment erosion in stay vane is lower than guide vane and runner, whereas the highest values of the erosion intensity occurs in the runner. The sediment erosion due to fine solid particles in the turbine is mainly resulted from cutting. However, high sediment erosion due to deformation is also produced at the leading edges of stay vane and guide vane.

***Keywords*:** Hydroelectric Power, Francis Turbine, Liquid-Solid Two Phase Flow, Sediment Erosion.

1. Introduction

Sediment erosion in Francis turbines is a mechanical wear produced in flow components due to the presence of the solid particles in the rivers [1]. This material destruction in hydropower equipment leads to a low efficiency and affects operating reliability [2].Thus, it is important to develop the effective method for predicting sediment erosion so as to improve this severe situation.

Numerical prediction of sediment erosion based on computational fluid dynamics (CFD) is a powerful tool, in which the turbulence modeling plays an important role to determine the motion and dispersion of the solid particle [3]. For most engineering applications, Reynolds-Average Navier-Stokes (RANS) method is preferable because sediment erosion involves in complicated two-phase flow. Some researchers studied sediment erosion phenomenon using RANS solution with k-ε turbulence model [1,6,7], while few studies predicted the sediment erosion in Francis turbines using RANS method based on k-ω *SST* turbulence model[2,4,5]. The result comparisons between two turbulence models indicate that no remarkable differences can be observed except the velocity profiles near wall. Generally, RANS method shows limited resolution to determine the motion of solid phase affected by flow fluctuations [4] and some modifications are necessary to reduce the over-estimated eddy viscosity of the liquid phase [9,10]. That means attention must be paid to develop non-conventional turbulence models to improve the accuracy with suitable computational resource.

The desirable method for turbulent flow prediction is to solve the fluctuation features with possibly lowest cost. In recent years, partially average Navier-Stokes (PANS) method has been used instead of the conventional RANS method. PANS is a bridge from RANS to Direct Numerical Simulation (DNS), where two parameters quantify the resolution level: the

unresolved-to-total ratios of turbulence kinetic energy (f_k) and dissipation (f_ε) [6]. The method predicted accurate physics in the flow over a backward-facing step [5], a cylinder [7] and a hydrofoil [8]. Therefore, it is evident that PANS is suitable for predicting complex turbulence behavior of large scale unsteadiness. Though PANS shows excellent improvements to predict cavitating turbulent flows[14,15,16], there is no information regarding the prediction of liquid-solid two phase flow and sediment erosion by applying this method.

Inspired by their work, the present paper uses a modified PANS model proposed by Huang et al.[5] to improve the three-dimensional numerical simulation of the liquid-solid two phase flow in a model Francis turbine, along with sediment erosion prediction of main flow components.

.

2. Numerical Method

The present numerical simulation uses a modified PANS model based on the Eulerian approach, coupled with Lagrangian approach for the dispersed phase. A commercial CFD code, ANSYS FLUENT 15.0, is used to solve the equations. The modified Partially-Averaged Navier-Stokes model has been implemented via user defined functions. The solid particle injection is applied using the disperse particle method (DPM) with scholastic tracking and Discrete Random Walk model (DRW) to predict the dispersion of particles, due to velocity fluctuation in the liquid phase. The continuity and momentum control equations for continuous phase and discrete phase are introduced in literature [12]. For continuous phase, the government equations do not consider variations in density due to the cavitation phenomenon. The following are main equations for this study.

2.1. Turbulence Model

The original PANS turbulence model proposed by Girimaji [6] is derived from k-ε turbulence model, in which two parameters, the unresolved-total ratios of kinetic energy f_k (k_u/k) and dissipation f_ε ($\varepsilon_u/\varepsilon$), are used in the calculation of the turbulence viscosity given in Eq. (1). The subfilter scale stress is modeled with the Boussinessq constitutive approximation.

$$\mu_t = C_\mu \rho \frac{k_u^2}{\varepsilon_u}, \tag{1}$$

In this study, the modified PANS model proposed by Huang [5] is used, where f_k-field is dependent on timely and spatial flow information. The turbulence model is shown as follows:

$$\frac{\rho \partial (u_i k_u)}{\partial x_i} = P_u - \rho \varepsilon_u + \frac{\partial}{\partial x_j}\left[(\mu + \frac{\mu_t}{\sigma_{ku}}) \left(\frac{\partial k_u}{\partial x_j} \right) \right], \tag{2}$$

$$\frac{\rho \partial (u_i \varepsilon_u)}{\partial x_i} = \frac{\partial}{\partial x_j}\left[(\mu + \frac{\mu_t}{\sigma_{\varepsilon u}}) \left(\frac{\partial \varepsilon_u}{\partial x_j} \right) \right] + C_{\varepsilon 1} P_u \frac{\varepsilon_u}{k_u} - C^*_{\varepsilon 2} \frac{\varepsilon_u^2}{k_u}, \tag{3}$$

where u is the velocity. ρ is the density. p is the pressure. μ is the dynamic viscosity. μ_t is the turbulent viscosity. P_u is the unresolved production term. The model coefficients σ_{ku}, $\sigma_{\varepsilon u}$ and $C^*_{\varepsilon 2}$ are determined the follow equation:

$$\sigma_{ku} = \sigma_k \frac{f_k^2}{f_\varepsilon}, \sigma_{\varepsilon u} = \sigma_\varepsilon \frac{f_k^2}{f_\varepsilon}, C^*_{\varepsilon 2} = C_{\varepsilon 1} + \frac{f_k}{f_\varepsilon}(C_{\varepsilon 2} - C_{\varepsilon 1}), \tag{4}$$

where the empirical constants are proposed by Launder and Spalding [13]: $C_{\varepsilon 1}$=1.44, $C_{\varepsilon 2}$=1.92, σ_k=1.0, σ_ε =1.3. The unresolved-to-total ratio $f\varepsilon$ ($\varepsilon_u/\varepsilon$) is set to 1.0, due to the flow in all domains is characterized by high Reynolds number.

The unresolved-to-total ratio f_k (k_u/k) sets the cut-off between resolved and unresolved scales for controlling the flow resolution. For evaluating f_k that can be support at a given mesh and turbulence length, Eq. (5) has been used.

$$f_k = \min(1, \mathrm{C}_{\mathrm{PANS}}(\Delta / l)^{2/3}), \tag{5}$$

where l is the turbulence length scale ($l=k^{1.5}/\varepsilon$). Δ is the local averaged grid dimension $\Delta=(\Delta x \cdot \Delta y \cdot \Delta z)^{1/3}$.To improve the physical resolution of the turbulence model, $\mathrm{C}_{\mathrm{PANS}}$ is discussed using Eq. (6).

$$\mathrm{C}_{\mathrm{PANS}} = 1/\left(\mathrm{C}_{\mathrm{m}}\sqrt{C_\mu}\right), \tag{6}$$

where the constant C_μ=0.09. $\mathrm{C_m}$ is a coefficient related to the difference between the smallest and the averaged grid dimension depends on the ratio of grid dimension generated in each case of analysis.

Table 1 shows a comparison with different $\mathrm{C_m}$ value for predicting hydraulic performance of a Francis turbine, whose geometry and performance are explained in the literature [14]. The data for numerical simulation are marked with "Num", and the tested data are marked with "Exp.". For convenience, the hydraulic efficiency of the turbine is calculated using Eq. (7).

$$\eta_{\mathrm{h}} = M \cdot \omega / (\rho g Q H), \tag{7}$$

where M is the torque acting on turbine runner and H is the head given by Eq. (8). ω is the angular speed. Q is the discharge. g is the gravitational acceleration.

$$M = Z_{\mathrm{b}}\left(\int (r \times (\tau . N))\mathrm{d}A\right).\mathrm{i}_{\mathrm{z}} \tag{8}$$

where A represents surface comprising the rotating parts of the runner.τ is stress tensor. N is the unit normal vector to the surface. r is the position of the vector respect to the point zero, placing in the top and center of the runner. $\mathrm{i_z}$ is the unit vector along the axis of rotation.

Table 1: Turbine performance predicted by modified PANS.

Cases	$\mathbf{C_m}$	$\mathbf{C_{PANS}}$	$\boldsymbol{\eta_h}$ **/ %**	$\boldsymbol{Q_{nD}}$
Num1	1	3	92.34	0.693
Num2	2	1.5	92.57	0.693
Num3	3	1	93.03	0.692
Num4	6	0.5	94.04	0.691
Num5	7.5	0.4	93.76	0.691
Exp. data	-	-	94.54	0.686

It is noted that the prediction of hydraulic efficiency and discharge is dependent on the model coefficient. The coefficients proposed by Girimaji and Abdol-Hamid [15], i.e. $\mathrm{C_m}$=3 and $\mathrm{C_{PANS}}$=1, there are not small differences from the experimental data. Among those coefficients, $\mathrm{C_m}$=6 and $\mathrm{C_{PANS}}$=0.5 can yield better prediction accuracy.

2.2. Control Equation for Discrete Phase

Equation 9 based on Newton's second law is applied to calculate the velocity of each injected particle.

$$\frac{\partial (v_{\mathrm{p}})_i}{\partial t} = F_{\mathrm{D}i} + F_{\mathrm{p}i} + F_{\mathrm{B}i} + F_{\mathrm{m}i} + F_{Ci}, \tag{9}$$

where v_p is the particle velocity. F_{D}, F_{p}, F_{B}, F_{m} , F_{C} are the force of drag, pressure gradient, buoyancy, virtual mass and centrifugal forces.

In this study, the following assumptions are applied: the surrounding flow affects the particle motion, and the interaction between particles and Brownian motion are neglected. The particle shape is spherical and the physical properties of the solid phase are constant during the simulation. Particle distribution is estimated using Discrete Random Walk (DRW) model. The adequate number of particle injection is tracked repeatedly to generate a statistically meaningful sampling. Furthermore, the mass flow rate and exchange source terms for the particle injection are divided equally among multiple stochastic tracks.

2.3. Sediment Erosion Model

The sediment erosion over the wall surface produced by the solid particle is modeled as a function of the particle property and velocity, as well as wall surface property. Although the erosion mechanisms remain the same for gas-solid and liquid-solid erosion, previous studies conclude that the erosion model obtained using gas-liquid flow are not suitable for predicting the erosion produced by liquid-solid flow [16]. Further, some changes in the parameters can affect the accuracy of the estimations [17]. The present study applies the semi-empirical equations proposed by Desale et al. [18] as sediment erosion model. The equations are detailed in Eqs (10)-(13). The total erosion of a ductile material includes a contribution due to cutting and deformation.

The erosion rate due to deformation is calculated using the following relationship [19]:

$$E_D = E_{D90}.(\sin\gamma)^3, \tag{10}$$

where E_{D90} is the erosion rate at normal impact condition and γ is the incidence angle. It is assumed that the erosion wear at normal condition is caused only by deformation.

The erosion rate due to cutting E_C is predicted by:

$$E_C = E_0.f(\gamma).(\mathrm{MSF})^{-0.80}.(H_V)^{-0.72}.(v_p)^{2.35}.(d_p)^{1.55}.(C)^{-0.11}, \tag{11}$$

where C is the particle concentration. E_0 is an experimental coefficient. MSF is a mean shape factor. H_V is the hardness of the surface material in the Vickers scale. $f(\gamma)$ is the normalized function of the cutting erosion with impact angle γ, expressed by Eq. (12).

$$f(\gamma) = \begin{cases} (0.99)\left(\sin\left[(\pi/2)\left(\dfrac{\gamma}{\gamma_{max}}\right)\right]\right)^{0.58} & \gamma \le \gamma_{max} \\ (0.92)\sin\left[(\pi/2)-(\pi/2)\dfrac{(\gamma-\gamma_{max})}{(90-\gamma_{max})}\right]^{4.3} & \gamma > \gamma_{max} \end{cases}, \tag{12}$$

where $\gamma_{max}=0.55(H_V)^{0.69}$.

The angle for maximum erosion rate is 25.5 degree and the erosion at 90 degree is estimated considering only deformation erosion. From 0 to 25.5 degree, the erosion increases with the incidence angle. From 25.5 to 75 degree, the erosion decreases with the incidence angle. Finally, for incidence angles near 90 degree, the erosion slightly increases.

The total erosion rate E_T can be calculated by:

$$E_T = E_D + E_C, \tag{13}$$

Table 2 shows the averaged sediment erosion rate for different flow components in the turbine based on the prediction. The results indicate that the predicted sediment erosion is relatively stable for C_m=2~7.5. Among those coefficients, C_m=3 is also suitable for sediment erosion prediction**.**

Table 2: Averaged sediment erosion rate predicted using modified PANS with different coefficient [10^{-10} kg $m^{-2}s^{-1}$].

Cases	C_m	C_{PANS}	Stay vane	Guide vane	Runner
Num1	1	3	0.65	12.93	54.19
Num2	2	1.5	0.63	12.85	38.62
Num3	3	1	0.63	12.76	34.29
Num4	6	0.5	0.62	12.68	33.2
Num5	7.5	0.1	0.63	12.71	36.06

3. Geometry and Conditions

In this study, a model Francis turbine is used, its performance test has been conducted on a test rig at the Harbin Electric Company Ltd., China .The uncertainty of turbine efficiency is within 0.3%. Fig.1 shows the CFD computation domain, which consists of the model Francis turbine passages: spiral casing, stay vanes, guide vanes, runner and draft tube. The parameters for the model Francis turbine are listed in Table 3.

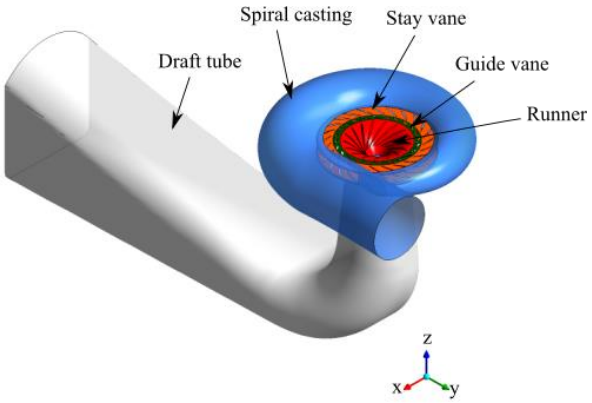

Fig. 1: Computation domain.

Table 3: Model turbine specification.

Parameter	Value
Runner inlet diameter, D (mm)	420
Runner blade number, Z_b	17
Relative height of the guide vane, b_0	0.18257
Guide vane number	24
Stay vane number	23

The operating condition for sediment erosion analysis is listed in Table 4. Note that the operation condition is near the best efficiency point for the turbine. The properties of the sand particles used in previous studies [12] was considered in the present study, and the detailed information is shown in the Table 5. Furthermore, the MSF (particle shape factor) is 1.0.

Table 4: Operating condition.

Parameter	Value	Equation according to IEC
Guide vane opening, α_0 /mm	16.7	
Specific speed, n_{QE}	0.686	$\omega Q^{0.5}H^{-0.75}$
Discharge coefficient, Q_{nD}	0.342	$Q\omega^{-1}D^{-3}$
Energy coefficient, E_{nD}	0.809	$H\omega^{-2}D^{-2}$
Speed factor, n_{ED}	1.110	$\omega DH^{-0.5}$

A structured mesh is generated throughout the computation domain, as shown in Fig. 2. Local refined mesh is applied in the region near guide vane, stay vane and runner blade to ensure that the first nodes away from the wall allow to match the y^+ values recommended for enhanced wall treatment. y^+ on the surface of the stay vane, guide vane and runner blade is less than 223.

For the mesh independent test, three mesh resolutions are considered. The differences between meshes are the number of nodes in the spanwise direction. Based on the results shown in Table 6, the medium resolution mesh with 2963290

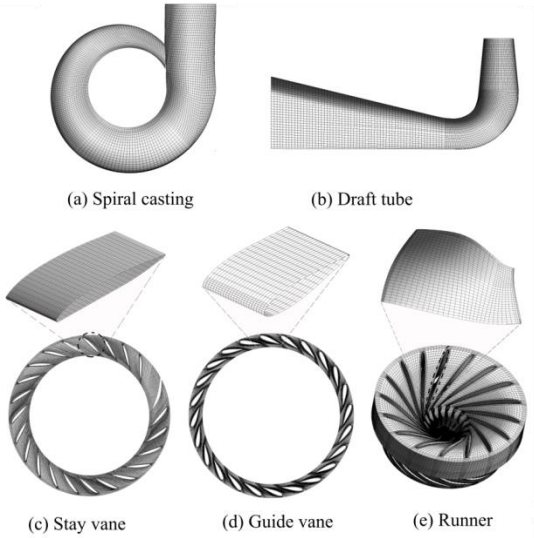

Fig. 2: Mesh generation of the calculation domain.

Table 5: Sediment flow characteristic.

Characteristic	Value
Mass flow rate /kg s^{-1}	0.4474
Density / kg m^{-3}	2650
Diameter /μm	62

nodes is selected to perform the simulation.

The numerical simulations have been carried out with all domains connected with the boundary conditions and coupling approach imposed as follows:

1. The total pressure is designated at the inlet of the spiral casing
2. A rotating frame is applied for the runner zone, and other regions are in a stationary frame.

3. Sliding mesh interfaces are created between: guide vane outlet flow surface and runner inlet flow surface, runner outlet flow surface and draft tube inlet flow surface.
4. Static pressure is designated at the outlet of the draft tube.
5. Solid walls are set as nonslip boundary conditions.

On the other hand, the solid phase injection is applied using Disperse particle method (DPM) at the domain inlet. Fully elastic collision is assumed at the walls. In previous studies of sediment erosion assessment[24, 25], the analysis of the adequate number of particle injection was carried out to generate a statistically meaningful sampling. Two hundred stochastic tracking tries ensure that erosion on the wall of turbine flow passage is independent of particle number.

Table 6: Results of the mesh independence test.

Cases	Nodes	η_h / %	Q_{nD}
Case 1 (coarse)	1197605	91.17	0.697
Case 2 (medium)	2963290	93.80	0.691
Case 3 (fine)	3459535	93.95	0.691
Exp. data	-	94.54	0.686

The steady state simulations are carried out using spatial derivatives discretized through Second Order Upwind scheme. Full pressure-velocity coupling is enabled using SIMPLE algorithm. Further, double precision is considered to improve the computation accuracy. A quantitative assessment about discharge difference was done in the interfaces between the fixed and rotating parts, which was lower than the order of 7.68×10^{-14} m^3 s^{-1}. In the same way, the difference between numerical solution and experimental data are lower than 6×10^{-3} m^3 s^{-1}.

4. Results and Discussion

4.1. Liquid Flow in Francis Turbine

Table 7 shows hydraulic efficiency and discharge predicted by the modified PANS model and standard *k-ε* turbulence model at BEF operation point. For comparison, the experimental data also is included. Though the predictions by both turbulence models agree well with experimental data for the discharge, a remarkable improvement for hydraulic efficiency prediction is observed by using the modified PANS model.

Table 7: Hydraulic efficiency and discharge predicted at BEP operation point.

Turbulence model	η_h / %	Q_{nD}
Standard *k-ε*	87.13	0.677
Modified PANS	93.80	0.691
Exp. data	94.54	0.686

4.2. Flow Prediction for Solid Phase

Since the erosion is governed by the velocity, incidence angle and concentration of the solid particles at the time of collision, the erosion prediction depends on the solutions of these parameters. The solid particle mass flow of 0.4474 kg/s, corresponding the volumetric concentration of C_v= 0.05% has been analyzed in the following.

4.2.1. Velocity Distribution

Figure 3 shows the flow field in the turbine. The velocity of liquid phase is plotted at the left side and that of the solid

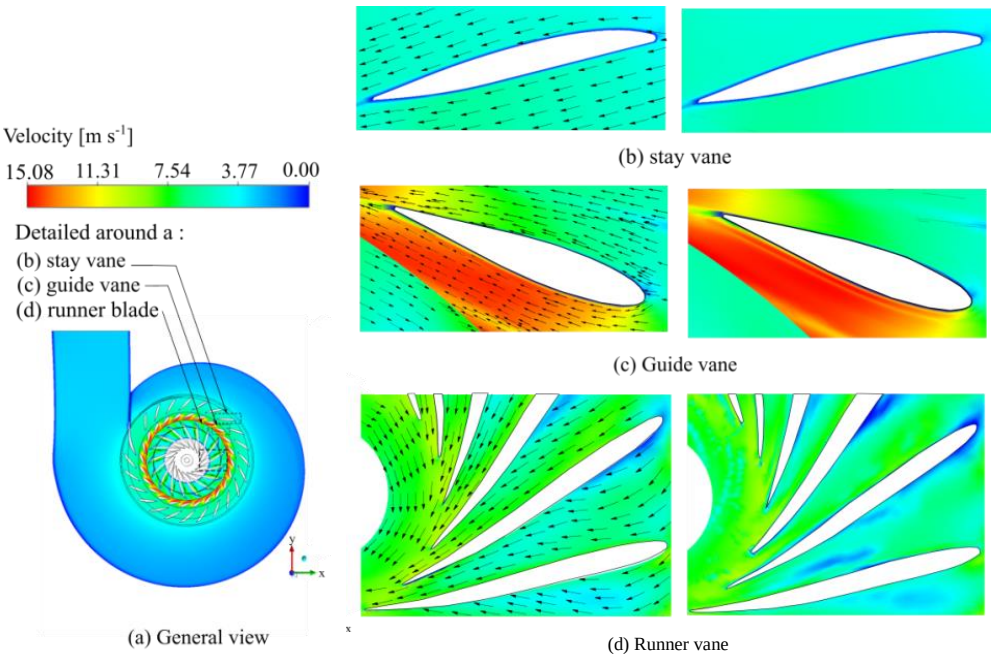

Fig. 3: Velocity distributions in flow components at BEP operation condition.

phase is at the right side. The results depict that velocity difference between particle and water is not large in the flow passage of Francis turbine. This agrees well with the previous studies of liquid-solid two-phase flow performed with fine particles [9, 26]. Near the runner blade, the velocity of solid phase is slower than that of liquid phase. Furthermore, the high velocity magnitude of the solid particle is near the suction surface of guide vane.

4.2.2. Incidence Angle

Figure 4(a) shows the incidence angle distribution of the solid phase over the vane surface of three flow components. The angle is calculated using Eq. (14) in an offset surface with a distance of half the height of the first cell.

$$\gamma = 90° - \cos^{-1}\left(\frac{N_1.v_{p1} + N_2.v_{p2} + N_3.v_{p3}}{v_p}\right), \tag{14}$$

where N_1, N_2 and N_3 are the unit normal vector along axis x, axis y and axis z respectively. v_{p1},v_{p2} and v_{p3} are the particle velocity in x, y and z direction, calculated using Eq. (9). The vector considered for calculations in a surface cell is normal to the center of the surface. The results show that the leading edge of the guide vane and stay vane receives the impact of the solid particle in almost perpendicular direction, while the incidence angle acting on the pressure side of the guide vane and stay vane is lower than the angle for maximum erosion wear (γ_{max}= 25.5°) which are between 7 and 12 degree. Furthermore, the solid particle impacts to the runner blade pressure side near the trailing edge with angles close to the angle of maximum erosion and with values higher, between 26 and 62 degree. Near the runner band, the incidence angle is larger.

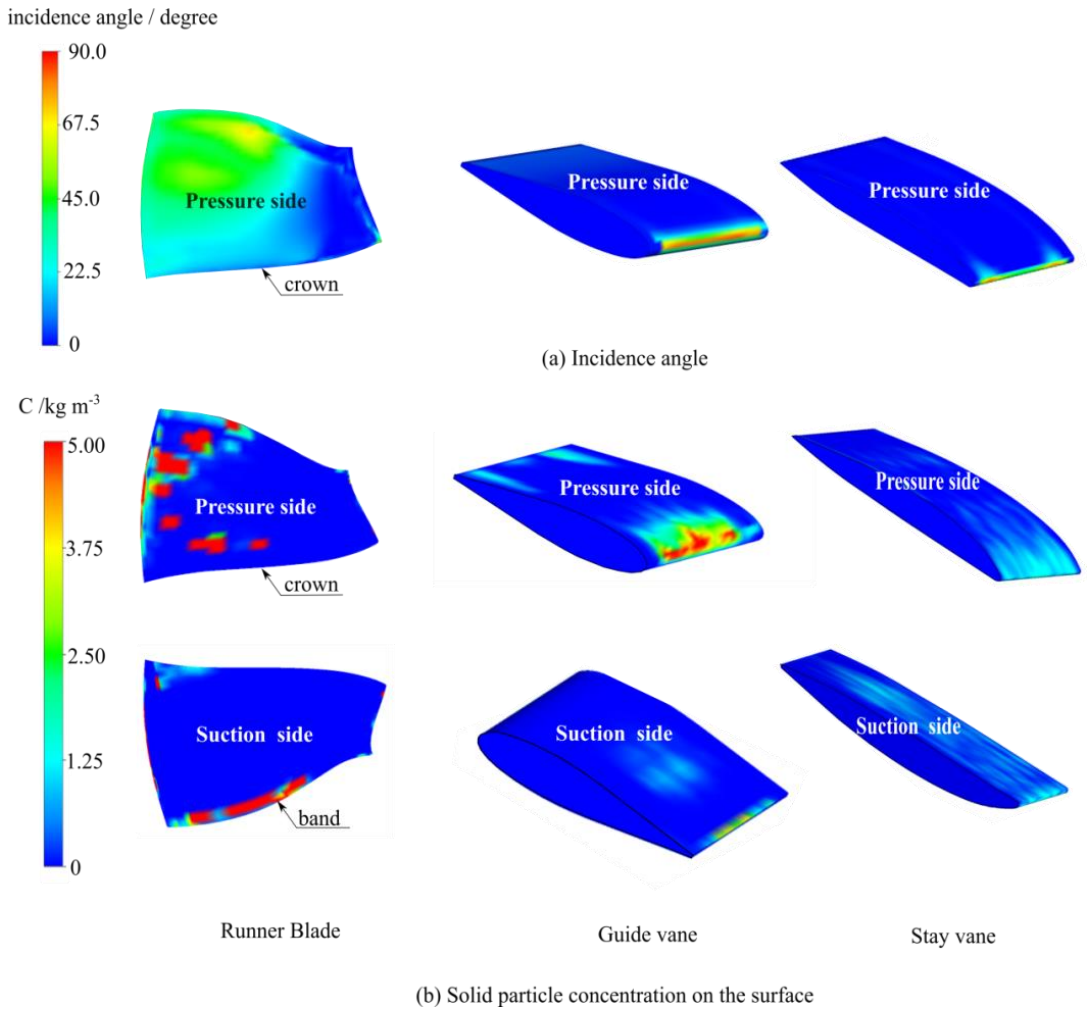

Fig. 4: Solid phase flow characteristic near typical vanes at BEP operation condition.

4.2.3. Particle Concentration

The volume fraction of solid particle near the passage wall provides an important guideline to locate potential areas of sediment erosion [3]. The concentration contour of solid particle over the vane/blade is shown in Fig. 4 (b). Generally, the concentration on the suction side is less than that on the pressure side of vane/blade. The numerical results indicate that the concentration is high at the leading edge of guide vane, and the areas with high concentration are not continuous on the pressure side of the runner blade. On the suction side near the runner band, the concentration is not small.

4.3. Sediment Erosion Prediction

4.3.1. Effect of Turbulence Model

Table 8 shows the average sediment erosion rate prediction for runner, guide and stay vane using aforementioned

Table 8: Averaged sediment erosion rate predicted using different turbulence models at BEP operation condition [unit: 10^{-10} kg $m^{-2}s^{-1}$].

Turbulence model	Stay vane	Guide vane	Runner
Standard k-ε	1.52	31.7	221.1
Modified PANS	0.62	12.68	33.2

turbulence models. It is noted that the modified PANS model leads to much smaller sediment erosion rate. The difference of the sediment erosion prediction between modified PANS and standard k-ε turbulence model is due to the estimation of velocity difference between two phases [8,21,27], which is dependent on both turbulence model and dispersion particle model. Similarly, previous studies of sediment erosion show that a better accuracy to capture the eddies reduces the erosion rate estimation, when y^+ are defined with recommended values [25].

4.3.1. Sediment Erosion

Figure 5 shows the sediment erosion distribution using modified PANS in runner blades (right side), stay vanes (left side) and guide vanes (center). The figures identify the areas of high erosion. The red color indicates the highest value of erosion intensity, whereas a blue color denotes the lowest erosion intensity. Cutting, deformation and the total sediment erosion rates are shown in Fig. 5(a), 5(b) and 5(c) respectively.

Based on the results, the following characteristics can be seen when the Francis turbine is operated at the design point:

1. As shown in Fig. 5(c), the total sediment erosion over stay vanes is lower than that over guide vane and runner, whereas the higher intensity occurs in the runner. The highest values of the erosion intensity are located in scatted regions of the pressure side near the trailing edge of the runner blade. Previous studies[1,2,24] have also shown the same situation. It is remarkable that there is no sediment erosion on the suction side of guide vane.

2. The sediment erosion in the aforementioned components is mainly produced by cutting. On the suction side, there is severe sediment erosion on the runner band, and scattered sediment erosion occurs near the trailing edge of stay vane. However, a high contribution of sediment erosion at leading edge of the guide vane and stay vane occurs due to deformation as shown in Fig. 5(b).

3. The sediment erosion has different location for different flow component. For the runner, scattering areas of sediment erosion occurs on the pressure side and suction side near the band. Erosion due to cutting is more predominant than deformation; for the guide vane, a high sediment erosion rate occurs at two main areas on pressure side: the region near the trailing edge and the leading edge. The erosion near the trailing edge is produced by cutting and the erosion at the leading edge is a combination of cutting and deformation produced by high solid particle concentration and perpendicular impact angle by solid particle; for the stay vane, sediment erosion is produced at the leading edge and scattered areas on suction side near the trailing edge. The erosion intensity at the vane leading edge is higher. Both areas are affected by cutting as show in Fig. 5(a). Furthermore, a great deformation erosion contribution is produced at the leading edge, as observed in Fig. 5(b).

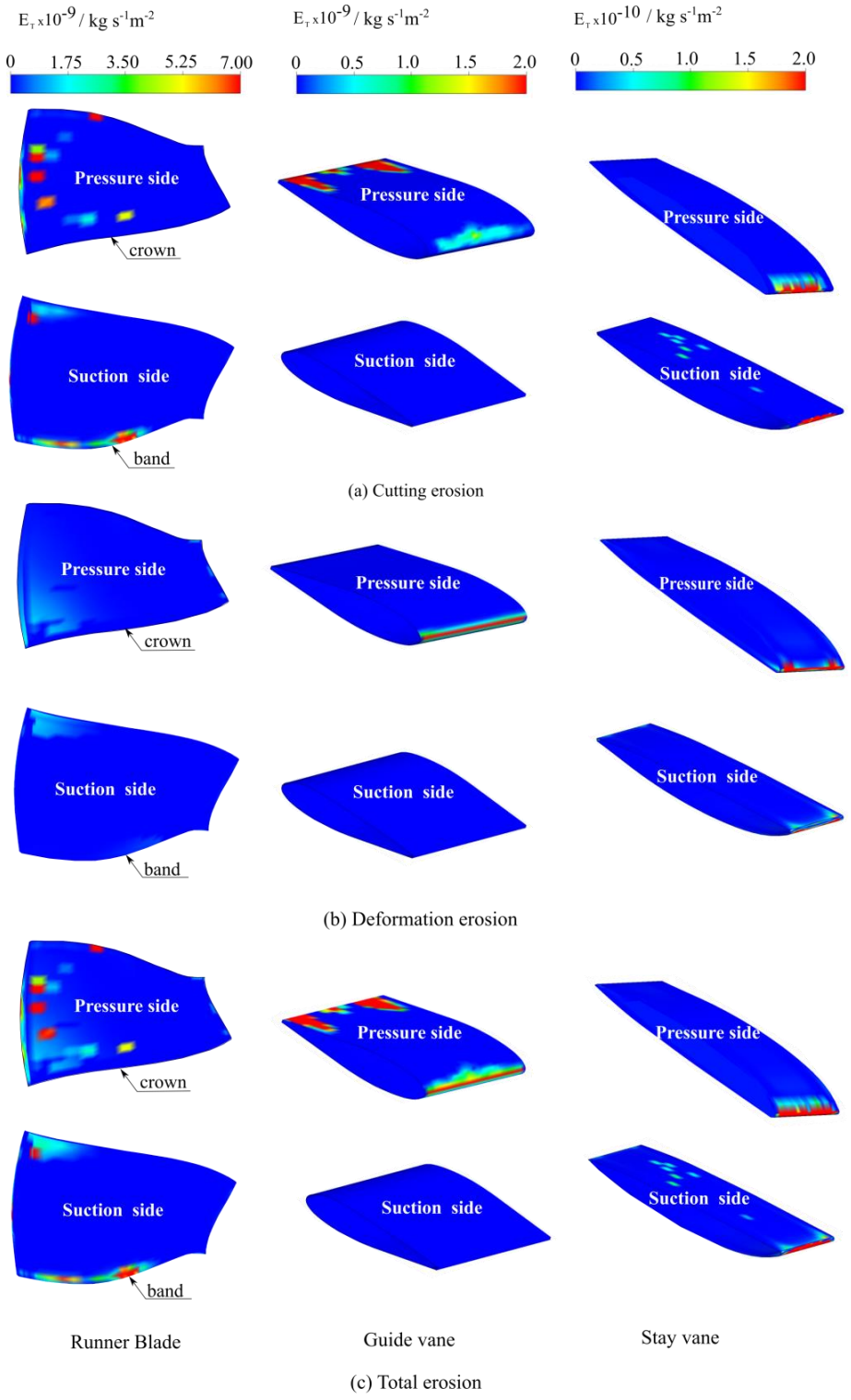

Fig. 5: Sediment erosion on the surface of typical vanes at BEP operation condition.

5. Conclusions

In this study, a modified PANS model was applied to the three-dimensional numerical simulation of liquid flow in Francis turbine. The unresolved-to-total ratio of turbulence kinetic energy, f_k, was decided considering the difference between local average grid size and the smallest grid size. The present calculation successfully predicted the hydraulic performance such as discharge and turbine efficiency of the turbine based on the comparison with the experiment. The solid particle flow predictions were carried out using Lagrangian approach and disperse particle method. The sediment erosion in main flow components of the turbine was estimated using an appropriate erosion model.

1. Based on the results of the present study, the following conclusions can be drawn:

Higher physical resolution captured by the turbulence model cause a diminution of the sediment erosion prediction.

2. Sediment erosion in stay vanes is lower than guide vane and runner blade, whereas the higher intensity occurs in the runner.

3. Sediment erosion in stay vane, guide vane and runner are mainly produced by cutting. However high deformation erosion is produced at the leading edges of stay vane and guide vane.

Acknowledgments

This work was supported by the National Natural Science Foundation of China (Grants No. 51776102), Beijing Natural Science Foundation (3182014), the Major National Scientific Instrument and Equipment Development Project (No. 2011YQ07004901), and State Key Laboratory of Hydroscience and Engineering (Project No. sklhse-2017-E-02). This work also was partially funded by the Secretaría de Educación Superior, Ciencia y Tecnología (SENESCYT) of Ecuador.

References

[1] H. Neopane, "Sediment erosion in hydro turbines," Norwegian University of Science and Technology, 2010.

[2] G. Peng, Z. Wang, Y. Xiao, and Y. Luo, "Abrasion predictions for Francis turbines based on liquid-solid two-phase fluid simulations," *Eng. Fail. Anal.*, vol. 33, pp. 327–335, 2013.

[3] S. Huang, X. Su, and G. Qiu, "Transient numerical simulation for solid-liquid flow in a centrifugal pump by DEM-CFD coupling," *Eng. Appl. Comput. Fluid Mech.*, vol. 9, no. 1, pp. 411–418, 2015.

[4] A. Guha, "Transport and Deposition of Particles in Turbulent and Laminar Flow," *Annu. Rev. Fluid Mech.*, vol. 40, no. 1, pp. 311–341, 2008.

[5] R. Huang, X. Luo, B. Ji, and Q. Ji, "Turbulent flows over a backward facing step simulated using a modified Partially-Averaged Navier-Stokes model," *J. Fluids Eng.*, vol. 139, no. 4, p. 7, 2016.

[6] S. S. Girimaji, "Partially-Averaged Navier-Stokes Model for Turbulence: A Reynolds-Averaged Navier-Stokes to Direct Numerical Simulation Bridging Method," *J. Appl. Mech.*, vol. 73, no. 3, p. 413, 2006.

[7] S. Lakshmipathy and S. S. Girimaji, "Partially Averaged Navier–Stokes (PANS) Method for Turbulence Simulations: Flow Past a Square Cylinder," *J. Fluids Eng.*, vol. 132, no. 12, p. 121202, 2010.

[8] J. Liu, Z. Zuo, Y. Wu, B. Zhuang, and L. Wang, "A nonlinear Partially-Averaged Navier-Stokes model for turbulence," *Comput. Fluids*, vol. 102, pp. 32–40, 2014.

[9] B. Ji, X. Luo, Y. Wu, X. Peng, and H. Xu, "Partially-Averaged Navier-Stokes method with modified k-?? model for cavitating flow around a marine propeller in a non-uniform wake," *Int. J. Heat Mass Transf.*, vol. 55, no. 23–24, pp. 6582–6588, 2012.

[10] R. Huang, X. Luo, and B. Ji, "Numerical simulation of the transient cavitating turbulent flows around the Clark-Y hydrofoil using modified Partially Averaged Navier-Stokes method," *J. Mech. Sci. Technol.*, vol. 31, no. 6, pp. 2849–2859, 2017.

[11] H. Foroutan and S. Yavuzkurt, "A partially-averaged Navier-Stokes model for the simulation of turbulent swirling flow with vortex breakdown," *Int. J. Heat Fluid Flow*, vol. 50, pp. 402–416, 2014.

[12] E. Cando, A. Yu, L. Zhu, J. Liu, L. Lu, V. Hidalgo, and X. Luo, "Unsteady numerical analysis of the liquid-solid two phase flow around a step using Eulerian-Lagrangian and the filter-based RANS method," *J. Mech. Sci. Technol.*, vol. 31, no. 6, pp. 2781–2790, 2017.

[13] B. E. Launder and D. B. Spalding, "The numerical computation of turbulent flows," *Comput. Methods Appl. Mech. Eng.*, vol. 3, no. 2, pp. 269–289, 1974.

[14] X. Luo, A. Yu, B. Ji, Y. Wu, and Y. Tsujimoto, "Unsteady vortical flow simulation in a Francis turbine with special emphasis on vortex rope behavior and pressure fluctuation alleviation," *Proc. Inst. Mech. Eng. Part A J. Power Energy*, vol. 231, no. 3, pp. 215–226, 2017.
[15] S. Girimaji and K. Abdol-Hamid, "Partially-Averaged Navier Stokes Model for Turbulence: Implementation and Validation," *43rd AIAA Aerosp. Sci. Meet. Exhib.*, no. January, pp. 1–14, 2005.
[16] A. Levy, *Solid Particle Erosion and Erosion Corrosion of Materials*. Ohio, USA: ASM International Publication, 1995.
[17] M. Parsi, K. Najmi, F. Najafifard, S. Hassani, B. S. McLaury, and S. A. Shirazi, "A comprehensive review of solid particle erosion modeling for oil and gas wells and pipelines applications," *J. Nat. Gas Sci. Eng.*, vol. 21, pp. 850–873, 2014.
[18] G. R. Desale, B. K. Gandhi, and S. C. Jain, "Development of Correlations for Predicting the Slurry Erosion of Ductile Materials," *J. Tribol.*, vol. 133, no. 3, p. 31603, 2011.
[19] J. H. Neilson and A. Gilchrist, "Erosion by a stream of solid particles," *Wear*, vol. 11, no. 2, pp. 111–122, 1968.
[20] M. A. Nemitallah, R. Ben-Mansour, M. A. Habib, W. H. Ahmed, I. H. Toor, Z. M. Gasem, and H. M. Badr, "Solid Particle Erosion Downstream of an Orifice," *J. Fluids Eng.*, vol. 137, no. 21302, pp. 1–11, Sep. 2014.
[21] P. Frawley, P. O'Mahony, and M. Geron, "Comparison of Lagrangian and Eulerian Simulations of Slurry Flows in a Sudden Expansion," *J. Fluids Eng.*, vol. 132, no. 9, p. 91301, 2010.
[22] A. Yu, B. Ji, R. F. Huang, Y. Zhang, Y. N. Zhang, and X. W. Luo, "Cavitation shedding dynamics around a hydrofoil simulated using a filter-based density corrected model," *Sci. China Technol. Sci.*, vol. 58, no. 5, pp. 864–869, 2015.
[23] D. Liu and M. Yang, "Research of Liquid-Solid Two Phase Flow in the Chemical Pump," *Adv. Water Resour. Hydraul. Eng.*, pp. 2203–2207, 2009.
[24] C. T. Crowe, T. R. Troutt, and J. N. Chung, "Numerical Models for Two-Phase Turbulent Flows," *Annu. Rev. Fluid Mech.*, vol. 28, no. 1, pp. 11–43, 1996.
[25] Eltvik Mette, "Sediment erosion in Francis turbines," Norwegian University of Science and Technology, 2013.
[26] R. Koirala, B. Thapa, H. P. Neopane, B. Zhu, and B. Chhetry, "Sediment erosion in guide vanes of Francis turbine: A case study of Kaligandaki Hydropower Plant, Nepal," *Wear*, vol. 362–363, pp. 53–60, 2016.